Velocity Field in a Vertical Foam Film

Jacopo Seiwert,[1,2] Ronan Kervil,[1,3] Soniraks Nou,[1] and Isabelle Cantat[1]
[1]UMR 6251 CNRS/Université de Rennes 1, 35042 Rennes Cedex, France
[2]Air Liquide, Centre de Recherche Paris-Saclay, Les Loges-en-Josas, France
[3]ILM, UMR5306 Université Claude Bernard Lyon 1—CNRS, Université de Lyon, 69622 Villeurbanne, France
(Received 19 July 2016; revised manuscript received 13 November 2016; published 27 January 2017)

The drainage of vertical foam films governs their lifetime. For a foam film supported on a rectangular solid frame, when the interface presents a low resistance to shear, the drainage dynamics involves a complex flow pattern at the film scale, leading to a drainage time proportional to the frame width. Using an original velocimetry technique, based on fluorescent foam films and photobleaching, we measure the horizontal and vertical components of the velocity in a draining film, thus providing the first quantitative experimental evidence of this flow pattern. Upward velocities up to 10 cm/s are measured close to the lateral menisci, whereas a slower velocity field is obtained in the center of the film, with comparable downwards and horizontal components. Scaling laws are proposed for all characteristic velocities, coupling gravitational effects, and capillary suction.

DOI: 10.1103/PhysRevLett.118.048001

The gravity drainage of a foam film governs its thinning and its ultimate rupture and is thus a key factor in foam stability. A vertical thin film of pure liquid breaks into droplets and disappears in a fraction of second. In foam films, surfactants ensure the stability with respect to hole formation but are also at the origin of a surface tension gradient, i.e., a Marangoni force, which balances the film weight [1,2]. In their seminal work, Mysels, Shinoda, and Frankel [1] distinguished two kinds of drainage, associated to foaming solutions producing either rigid or mobile interfaces. The rigid ones can resist to in-plane shear stress and thus remain static during drainage. Consequently, a Poiseuille flow, driven by the gravity g, develops between the interfaces with a typical velocity, known as the Reynolds velocity, scaling as $v_R = \rho g h_0^2/\eta$, where ρ and η are, respectively, the density and the viscosity of the aqueous solution and h_0 is the thickness of the film. When $h_0 = 3$ μm, $v_R \approx 100$ μm/s. Mobile interfaces, in contrast, can deform and flow. However, Mysels, Shinoda, and Frankel still assume that the interface area is locally conserved: The mobile interfaces are described as an inextensible two-dimensional liquid with an interface shear viscosity η_s. In this latter case, drainage is much faster and the velocity of the fluid is close to the interface velocity. Because of its low resistance to shear, complex instabilities can develop in the film, as marginal regeneration [3–5] or 2D turbulence [6–8].

For mobile films, the typical drainage time is proportional to the film width [1,3], which is a clear experimental signature of a drainage dominated by lateral boundary effects. Close to the meniscus connecting a thin film to a solid frame, the interface curvature, and the resulting Laplace pressure, are non-negligible and induce a pressure-driven flow from the film toward the meniscus. This phenomenon produces a pinching of the film along the menisci with both rigid [9] or mobile interfaces [5,10]. In the case of vertical films with mobile interfaces, these film thickness inhomogeneities are unstable in a gravity field [11–13]: The thinnest parts, at the edge of the film, move upwards, while the thickest ones, in the center of the film, move downwards. This results in a net volume flux downwards, which has been conjectured by Mysels, Shinoda, and Frankel to dominate the drainage process for mobile films [1].

In this Letter, we measure the velocity field in such a vertical mobile film, and we provide the first quantitative measurement of the horizontal component of the velocity, which is shown to be of the same order of magnitude as the vertical one. On the basis of the ideas developed by Mysels, Shinoda, and Frankel, which, to our best knowledge, never led to quantitative predictions, we build original scaling laws for both the upward and the downward velocities.

The film thickness can be precisely measured by interferometry, and its time evolution provides some information on the fluid velocity [14–16]. However, only the component normal to the thickness gradient is available. An alternative is to use tracers [17,18], but they slightly deform the film which, in a vertical film, leads to artifactual gravity-induced motion. Here, we propose a novel technique, based on fluorescent labeling of the flow, which overcomes these drawbacks. Our surfactant solution is made of 10 g/L sodium dodecyl sulfate (SDS), 0.1 g/L fluorescein sodium, and 10% wt glycerol in pure water. The equilibrium surface tension is $\gamma = 37$ mN/m, the bulk viscosity $\eta = 1.3$ mPa $\cdot$ s, and the density $\rho = 10^3$ kg/m^3. Films are created on a vertical metallic frame of thickness 1 mm and internal width $2W$. The frame is withdrawn from the solution at a constant speed

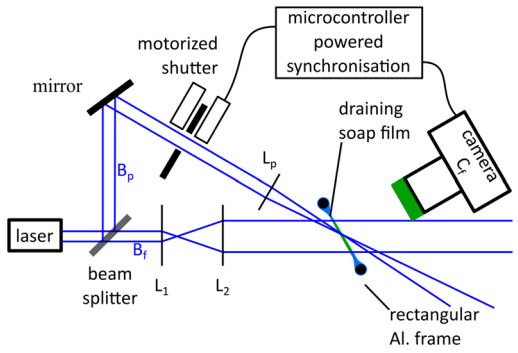

FIG. 1. Sketch of our experimental setup.

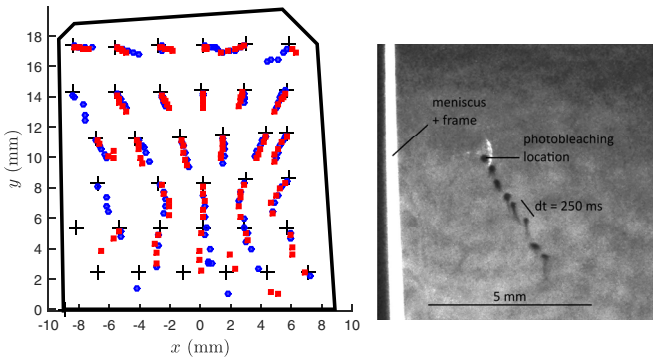

FIG. 2. (Left) Streak lines recorded just after $t = 1$ s, visualized with the photobleached spots produced every 250 ms from $t = 0$ to $t = 1$ s (so five spots) at the location marked with +. The thick black line represents the frame supporting the film. Spots coming from different photobleaching locations have been recorded on a different film. For each location, two spot series are shown (filled circle and filled square), obtained on two different films, thus evidencing the very good reproducibility of the flow, except for the bottom of the film. (Right) Example of an experimental image of photobleached spots.

$U_0 = 5$ mm/s and stops at $t = 0$ when the film height reaches $H = 20$ mm. The film remains connected to the bath via a horizontal meniscus, oriented along the x axis. The y axis is vertical, with its origin at the level of the solution reservoir (see Fig. 2).

We first performed film thickness measurements for different frame widths (see Supplemental Material [19]) and evidenced a drainage time proportional to the frame width, characteristic of mobile interfaces. We then focused on the velocity measurements using the experimental setup shown in Fig. 1, with the $W = 10$ mm frame.

We use a 20 mW, 473 nm laser line, split into two parts B_f and B_p of equal power. Two convergent lenses of focal lengths 10 mm (L_1) and 200 mm (L_2) expand B_f to a diameter of approximately 20 mm, to excite the fluorescence over the whole film. This component is captured, with magnifications between 1 and 5, by a Nikon D7000 digital camera C_f fitted with the appropriate filter. The laser hits the film approximately 5° off from its perpendicular, which allows for C_f to be mounted strictly perpendicular to the film without being saturated by the incoming light.

The beam B_p, on the other hand, is reflected off an adjustable mirror and through a motorized shutter which pulses it. It is then focused on the film surface by a convergent lens (L_p) of focal length 100 mm: The light arriving at the film is intense enough to photobleach the fluorophore and thus produce a dark spot on the film. Depending on the experiment, we used 125 or 10 ms pulses, which created, respectively, 100 and 40 μm diameter spots. The shutter and the camera are synchronized with an accuracy of ± 3 ms.

We first focus on the central portion of the film. At a given location (x_{pl}, y_{pl}), we photobleached one dark spot (with a 125 ms pulse) every 250 ms from $t = 0$ and took one picture just after the laser pulse [see Fig. 2 (right)]. The spots remain well contrasted during a few seconds, although they travel over a distance much greater than their diameter. This proves experimentally that velocity gradients across the film are negligible, as we anticipated in the introduction. We repeated the experiment with different positions (x_{pl}, y_{pl}) of the photobleaching laser, with two series of measure at each location. We found a good reproducibility of the flow except for the series at the bottom of the film, since it is a region where the velocities are dominated by eddy circulations and are both much higher and more random. For each series, the position of all the spots visible at $t = 1$ s are reported in Fig. 2 (left), which shows the global structure of the flow.

At each time t, the distance between the last two spots gives a direct measure of the velocity at the location (x_{pl}, y_{pl}). The relative error on the velocity is mainly due to the spot size and is less than 10%. Its x and y components at $t = 1$ s are plotted in Fig. 3 for the same locations as in Fig. 2, except the lowermost line. At this time, the film thickness is 4.7 μm at $y = 9$ mm (see Supplemental Material [19]) and 1.6 μm at $y = 19$ mm (data not shown). In the following, orders of magnitude are obtained using $h_0 \sim 3$ μm. Both velocity components are of the order of 1 mm/s, which is 10 times larger than the Reynold velocity. For each height in the film, the x component has been fitted by a straight line. The fitting functions vanish at a position x_a close to 0 ($|x_a| < 0.3$ mm for every height), with a slope $\partial v_x/\partial x = -0.11 \pm 0.05$ s^{-1}, except for the lowest series where the slope is positive. The y component, on the other hand, is negative and roughly independent on x up to 2 mm from the edges. It increases (in magnitude) from top to bottom, and its mean value, given in the caption of Fig. 3 for each height y, is well fitted by the law $v_{\text{fit}}^{-}(y) = 0.22y - 4$ with y in millimeters and v_{fit}^{-} in mm/s.

The measure of the upward velocities close to the edges required a second series of experiments, with better spatial and temporal resolutions. Indeed, in this region of the film, velocities and velocity gradients are much higher. For these reasons, photobleached spots disappear within 100 ms

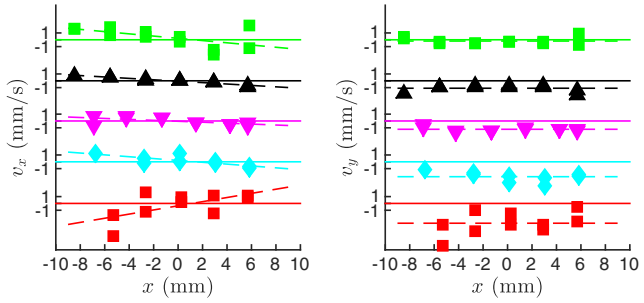

FIG. 3. x (left) and y (right) components of the fluid velocity within the film, at $t = 1$ s; the same data as in Fig. 2. Data are segregated by height in five series (5.4, 8.4, 11.4, 14.4, and 17.4 mm above the solution), indicated by horizontal lines. Data points are offset (vertically) from these base lines according to the value of the velocity. Dashed lines are straight line fits for the x component (from top to bottom, the slopes are $[-0.16; -0.1; -0.07; -0.13; 0.30]$ s^{-1}) and constant fits for the y component (from top to bottom: $[-0.19; -1.1; -1.2; -2.2; -2.9]$ mm/s).

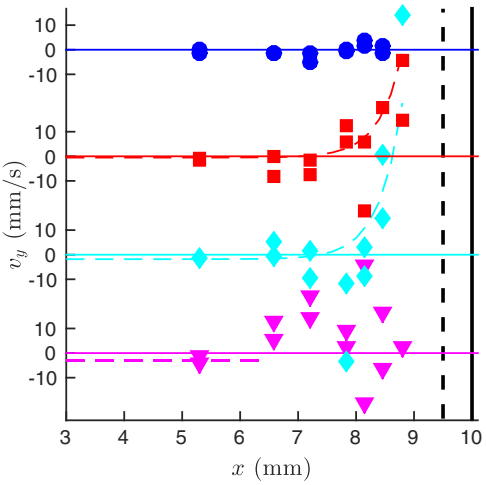

FIG. 4. y components of the fluid velocity, at $t = 1$ s, close to the right lateral meniscus (the same presentation as in Fig. 3, with a different set of data). Measurements are made 4, 10, 16, and 22 mm from the surface of the bath. The black vertical solid and dashed lines represent, respectively, the frame and the tip of the meniscus (i.e., the edge of the film). Colored dashed lines represent the function $v^-_{\rm fit}(y) + A\exp[(x - x_0)/\ell]$ given as a guide for the eyes, with $\ell = 0.5$ mm, $v^-_{\rm fit}(y)$ obtained from the data of Fig. 3, $x_0 = 8.5$ mm, and $A = [20\text{–}30]$ mm/s for $y = [10\text{–}16]$ mm. The relative error varies from less than 10% far from the meniscus to 50% for the data points with the highest velocities, very close to the meniscus.

and cannot be tracked over multiple images. Instead, we photobleach the spot with a 10 ms laser pulse and image the system 10–60 ms later, when the spot is still trackable. Its distance from the photobleaching location provides its velocity. Figure 4 shows the data from these measurements. The most striking result is a very large increase in the magnitude of the vertical velocity, from its characteristic downward value $v^- \sim 1$ mm/s to a characteristic upward value $v^+ \sim 20$ mm/s close to the meniscus. At the middle height of the film, the typical distance of variation can be estimated as $\ell \sim 0.5$ mm. This series of measurements is not as precise as the previous one, since in the worst cases the time of travel of the spot between creation and capture, the exposure time of the camera, and the duration of the laser pulse are of the same order (5–10 ms), leading to relative errors ranging from less than 10% to 50% as specified in the caption of Fig. 4.

The velocity field has been determined over the whole lifetime of the films, and vertical velocity values measured both in the middle of the film and close to the meniscus are plotted as a function of time in Fig. 5. The whole drainage process slowly decelerates with time while keeping a similar structure.

Because we measure both the horizontal and vertical velocities, we can determine for the first time the interface extension during the drainage process. In the central part of the film, the fits made in Fig. 3 lead to $\partial v_x/\partial x = -0.11 \pm 0.05$ s^{-1} and $\partial v_y/\partial y \approx 0.2 \pm 0.02$ s^{-1}. Our data thus evidence that $\mathrm{div}^{2D} v > 0$ and that some interface extension occurs. The two velocity derivatives are nevertheless of a similar order of magnitude (and opposite sign) in the whole film, except at the bottom of the film ($y < 6$ mm), where the derivative along y cannot be precisely measured. The prediction of the velocity field, taking into account this interface extension, would require an experimental determination of the coupling between the film extension and the dynamical surface tension. This is still an experimental challenge [20,21]. However, we believe that a model based on the original assumption of Mysels, Shinoda, and Frankel of an inextensible interface, as the one developed below, may capture a large part of the physics.

We consider the elementary piece of film $\mathcal{S}$ of area $dxdy$ and thickness $h(x, y)$, as depicted in Supplemental Material [19]. Its weight is $\rho g h \sim 3 \times 10^{-2}$ Pa, which determines the relevant order of magnitude for the forces. The Laplace pressure term and the inertial terms are both maximal in the pinched region, where they scale, respectively, as $\gamma h_0^2/\ell^3 \sim 3 \times 10^{-3}$ Pa, $\rho h_0 \partial v^+/\partial t \sim 3 \times 10^{-3}$ Pa, and $\rho h_0 (v^+)^2/H \sim 10^{-4}$ Pa (with $\partial v^+/\partial t \sim 1$ m/s^2 from Fig. 5). Both will be neglected in the following. As $\vec{v}$ is uniform across the film, only in-plane velocity derivatives are relevant, and these derivatives are independent on z. The viscous stress, integrated across the thickness of the film, thus becomes $\sigma^{2D}_{ij} = \eta^*(\partial v_i/\partial x_j + \partial v_j/\partial x_i)$ with i and j equal to x or y and $\eta^* = 2\eta_s + h\eta$. The term $h\eta$ is of the order of 3×10^{-9} Pa · s · m, which is much smaller than η_s [22]. It is thus neglected in the viscous force $\mathrm{div}^{2D}\sigma^{2D} \approx 2\eta_s \Delta^{2D}\mathbf{v}$ acting on $\mathcal{S}$.

With these assumptions, the equation of motion of $\mathcal{S}$ is given by $0 = 2\boldsymbol{\nabla}^{2D}\gamma + 2\eta_s\Delta^{2D}\mathbf{v} - \rho g h \mathbf{e}_y$. In the central part of the film, velocity gradients are small and the film

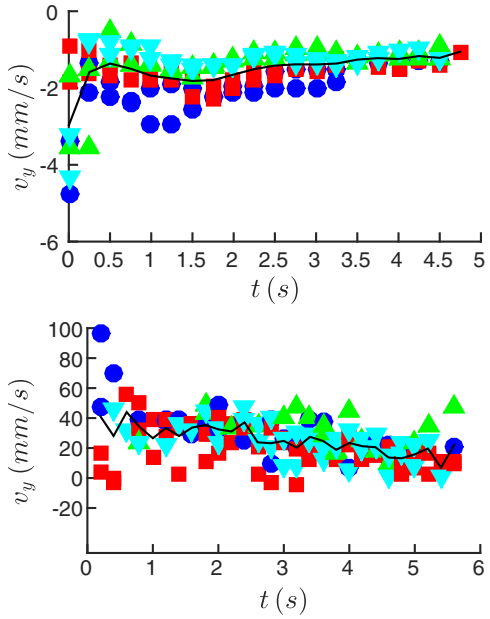

FIG. 5. Vertical component of the velocity as a function of time. Top figure: Film center, at the positions (in millimeters) filled circle ($x = 0.17$, $y = 8.3$), filled square (-2.7, 8.3), filled triangle (-1.4, 11.3), and filled inverted triangle (1.5,11.5). Bottom figure: Film right side filled circle (9.1,16) filled square (8.8,16), filled triangle (9.1,10), and filled inverted triangle (8.8,10). The solid black line is the mean value of all data sets.

weight is simply balanced by the surface tension gradient, which thus plays a dominant role in the dynamics. However, taking the curl of the previous equation and using the relation $\mathrm{div}^{2D} v = 0$ allows us to rewrite it without the variable γ:

$$2\eta_s \Delta^{2D}\Delta^{2D} v_y = \rho g \frac{\partial^2 h}{\partial x^2}. \tag{1}$$

Close to the meniscus, the film thickness is $h_m \ll h_0$ in a domain of width ℓ along the meniscus, and the derivative along x dominates. A simplified scaling relation can thus be deduced from Eq. (1): $\eta_s v^+/\ell^2 \sim \rho g \delta h$, with $\delta h = h_0 - h_m \sim h_0$. The downward velocity v^- at the same height is given by the conservation of the interface area in the domain between y and the top of the film, $v^+\ell + v^- W = 0$ (using $l \ll W$), leading to

$$v^- \sim -\frac{\rho g}{\eta_s}\frac{h_0 \ell^3}{W}. \tag{2}$$

Note that the downward volume flux across the horizontal line at position y is $v^+\ell h_m + v^- W h_0 \approx v^- W h_0$ (as $h_m \ll h_0$). This flux is at the origin of the film drainage.

Using the experimental values of ℓ and h_0 previously obtained, the predicted velocities are $v^+ \sim 20$ mm/s and $v^- \sim 1$ mm/s if $\eta_s \approx 4 \times 10^{-7}$ Pa · s · m. This value is of the same order as the value $\eta_s = 0.8 \times 10^{-7}$ Pa · s · m reported in Refs. [22,23] for the same SDS concentration.

The last unknown parameter in Eq. (2) is the pinch width ℓ. In the simpler case of a horizontal film of thickness h_0 put into contact, at the time $t = 0$, with a meniscus of radius r, the pinch characteristics scale at long time as $h_m \sim r(\tau/t)^{1/2}$ and $\ell \sim h_0(t/\tau)^{1/4}$, with $\tau = \eta h_0/\gamma$ [9]. In a vertical film, the dynamics can be schematized as follows: The large scale circulation brings a piece of film of thickness h_0 in contact with the lower part of the vertical meniscus; this piece of film then rises with the velocity v^+ along the meniscus and reaches the height y after a delay $t_d \sim y/v^+$. Inserting this time scale in the previous scaling, we predict $h_m \sim r(\tau v^+/y)^{1/2}$ and $\ell \sim h_0[y/(v^+\tau)]^{1/4}$. With $y = 1$ cm, we get the orders of magnitude $h_m^{th} \sim 100$ nm (with $r \sim 0.3$ mm) and $\ell^{th} \sim 0.2$ mm. This last value is consistent with $\ell \approx 0.5$ mm obtained in Fig. 4. Replacing ℓ in Eq. (2) allows us to propose finally a prediction for the drainage velocity in mobile foam films:

$$v^- \sim -\frac{h_0^2}{W}\left(\frac{\rho g \gamma y}{\eta_s \eta}\right)^{1/2}. \tag{3}$$

The orders of magnitude of our predictions for v^-, v^+, and ℓ are consistent with our experimental observations, as well as the scaling $v^- \sim 1/W$ and $v^+/v^- \sim -W/\ell$. We thus believe that the main physical ingredients have been captured by the model.

In conclusion, our technique allowed us to evidence a large scale recirculation in a draining foam film, with mobile interfaces. This technique also provides the first quantitative measurement of a film extension during drainage. Scaling laws for the different characteristic velocities are obtained with a simple model, based on the fact that the direct gravity drainage is negligible in comparison with the capillary drainage induced by the lateral meniscus. The gravity is nevertheless crucial, as it triggers the recirculation at the film scale, which constantly brings the thick film in contact with the lateral meniscus. This limits the film pinching and thus makes the capillary drainage much more efficient than in a horizontal film. A refined theoretical treatment of (i) the film extension and (ii) the coupling between the pinching process and the upward convection of the pinch would certainly improve our predictions. Qualitatively, the extension of the film interface induced by its own weight should increase the downward velocity in the central part of the film.

J. S., S. N., and R. K. acknowledge financial support from Agence Nationale de la Recherche (ANR-13-PDOC-0014-01-HYDROSURFDYN). We thank B. Mahé for some film thickness measurements, E. Gicquel, P. Chasle, and J.-C. Potier for technical support, and E. Rio, L. Champougny, and B. Dollet for fruitful discussions.

[1] K. J. Mysels, K. Shinoda, and S. Frankel, *Soap Films: Study of their Thinning and a Bibliography* (Pergamon, New York, 1959).
[2] P. G. de Gennes, Langmuir **17**, 2416 (2001).
[3] H. Stein, Adv. Colloid Interface Sci. **34**, 175 (1991).
[4] J.-L. Joye, G. J. Hirasaki, and C. A. Miller, Langmuir **10**, 3174 (1994).
[5] R. Bruinsma, Physica A (Amsterdam) **216**, 59 (1995).
[6] J. M. Chomaz, J. Fluid Mech. **442**, 387 (2001).
[7] H. Kellay, X.-l. Wu, and W. I. Goldburg, Phys. Rev. Lett. **74**, 3975 (1995).
[8] M. Winkler, G. Kofod, R. Krastev, S. Stöckle, and M. Abel, Phys. Rev. Lett. **110**, 094501 (2013).
[9] A. Aradian, E. Raphaël, and P.-G. de Gennes, Europhys. Lett. **55**, 834 (2001).
[10] H. Lhuissier and E. Villermaux, J. Fluid Mech. **696**, 5 (2012).
[11] V. Carrier, S. Destouesse, and A. Colin, Phys. Rev. E **65**, 061404 (2002).
[12] O. Pitois, N. Louvet, and F. Rouyer, Eur. Phys. J. E **30**, 27 (2009).
[13] N. Adami and H. Caps, Europhys. Lett. **106**, 46001 (2014).
[14] S. Berg, E. A. Adelizzi, and S. M. Troian, Langmuir **21**, 3867 (2005).
[15] G. Ropars, D. Chauvat, A. L. Floch, M. N. O'Sullivan-Hale, and R. Boyd, Appl. Phys. Lett. **88**, 234104 (2006).
[16] L. Saulnier, L. Champougny, G. Bastien, F. Restagno, D. Langevin, and E. Rio, Soft Matter **10**, 2899 (2014).
[17] J. Zhang, X. L. Wu, and N. Rashidnia, Phys. Fluids **18**, 085110 (2006).
[18] P. Petit, J. Seiwert, I. Cantat, and A.-L. Biance, J. Fluid Mech. **763**, 286 (2015).
[19] See Supplemental Material at http://link.aps.org/supplemental/10.1103/PhysRevLett.118.048001 for film thickness evolution and force balance on the film.
[20] L. Champougny, B. Scheid, F. Restagno, J. Vermant, and E. Rio, Soft Matter **11**, 2758 (2015).
[21] N. Adami and H. Caps, Phys. Rev. E **91**, 013007 (2015).
[22] P. Stevenson, J. Colloid Interface Sci. **290**, 603 (2005).
[23] A. Saint-Jalmes, Y. Zhang, and D. Langevin, Eur. Phys. J. E **15**, 53 (2004).